Geochemistry Geophysics Geosystems G3

Article
Volume 13, Number 1
18 April 2012
Q04006, doi:10.1029/2012GC004058
ISSN: 1525-2027

Published by AGU and the Geochemical Society

Slow slip events in Costa Rica detected by continuous GPS observations, 2002–2011

Yan Jiang and Shimon Wdowinski
Marine Geology and Geophysics, Rosenstiel School of Marine and Atmospheric Science, University of Miami, 4600 Rickenbacker Causeway, Miami, Florida 33129, USA (yjiang@rsmas.miami.edu)

Timothy H. Dixon
Department of Geology, University of South Florida, 4202 East Fowler Avenue, Tampa, Florida 33620, USA

Matthias Hackl
Department of Earth and Environmental Sciences, Ludwig Maximilians University, D-80333 Munich, Germany

Marino Protti and Victor Gonzalez
OVSICORI, Universidad Nacional Costa Rica, 2346-3000 Heredia, Costa Rica

[1] A network of continuously recording GPS stations has operated in the Nicoya Peninsula of northern Costa Rica since 2002. We processed all available data from this network for the period of 2002–2011 to investigate the occurrence of Slow Slip Events (SSE) on the subduction interface between the Cocos and Caribbean plates. In order to overcome signal masking by high levels of tropospheric noise, we developed a new technique that facilitates detection of transient events in the presence of noise. We identified five significant SSEs during the 2002–2011 period, with event middle times in 2003, 2005, 2007, 2009 and 2011, with an average recurrence interval of 21 $\pm$ 6 months. Time series analysis shows that transient deformation imparts a signature similar to random walk. Removal of the SSEs and regional common mode errors from the time series reduced velocity uncertainty by nearly an order of magnitude. Limited available data for the 2003, 2005 and 2011 events preclude detailed characterization of these events. However, good spatiotemporal coverage of the 2007 and 2009 events suggest that both events had irregular duration and distribution. In the 2007 event, slow slip started in the northwest coastal area and migrated southeastward over a period of $\sim$1 month. The 2009 event had a significantly longer event duration and larger surface displacement. Stations in the northwest area observed two separate SSEs in 2008.6 and 2009.4, correlating well with the tremor episodes offshore, indicating a shallow SSE slip patch with shorter recurrence interval. Significant differences between the 2009 and 2007 events lead us to question the simple recurrence interval model for the SSE in Nicoya.

Components: 9500 words, 10 figures, 3 tables.

Keywords: Costa Rica; GPS; SSE; subduction zones; tremor.

Index Terms: 1207 Geodesy and Gravity: Transient deformation (6924, 7230, 7240); 1209 Geodesy and Gravity: Tectonic deformation (6924); 1242 Geodesy and Gravity: Seismic cycle related deformations (6924, 7209, 7223, 7230).

Received 17 January 2012; **Revised** 12 March 2012; **Accepted** 16 March 2012; **Published** 18 April 2012.

Jiang, Y., S. Wdowinski, T. H. Dixon, M. Hackl, M. Protti, and V. Gonzalez (2012), Slow slip events in Costa Rica detected by continuous GPS observations, 2002–2011, *Geochem. Geophys. Geosyst.*, *13*, Q04006, doi:10.1029/2012GC004058.

1. Introduction

[2] Slow Slip Event (SSE) and seismic tremor are increasingly recognized as characteristic processes in many subduction plate boundaries [*Rogers and Dragert*, 2003; *Schwartz and Rokosky*, 2007; *Beroza and Ide*, 2011].These events may occur on a quasi-regular basis, referred to as Episodic Tremor and Slip events [*Rogers and Dragert*, 2003]. In Cascadia, such events typically last 1–4 weeks, have centimeters of slip on the plate interface and have recurrence intervals of 11 to 18 months [*Szeliga et al.*, 2008; *Schmidt and Gao*, 2010; *Holtkamp and Brudzinski*, 2010]. In Japan, episodic tremors and slip events vary in duration and distribution [*Obara*, 2010; *Liu et al.*, 2010]. The magnitudes and recurrence intervals of these events are important aspects of seismic hazard estimates [*Peng and Gomberg*, 2010; *Obara*, 2010]. To the extent that such events release a certain portion of accumulated strain due to plate motion on a locked plate interface, they may reduce the potential rupture area and magnitude of future large earthquakes. However they may also "load" adjacent segments of the interface [*Ito et al.*, 2007; *Segall et al.*, 2006].

[3] The Nicoya Peninsula is located in northwest Costa Rica, and overlies part of the Middle America subduction zone, where the Cocos plate subducts northeastward beneath the Caribbean plate (Figure 1) at a rate of ~85 mm/yr [*Dixon*, 1993; *DeMets*, 2001; *Outerbridge et al.*, 2010]. Plate convergence direction is 10° counter-clock wise from the trench- normal direction [*DeMets*, 2001]. The subduction rate in the trench-normal direction is 74–84 $mmyr^{-1}$ [*Outerbridge et al.*, 2010], while fore-arc motion is in the range of 8–14 $mmyr^{-1}$ [*DeMets*, 2001; *Norabuena et al.*, 2004; *LaFemina et al.*, 2009]. The subducting Cocos plate is formed at both the fast spreading East Pacific Rise (EPR), with relatively smooth seafloor topography, and the slow-spreading Cocos-Nazca Ridge (CNR), with relatively rough seafloor topography [*Protti et al.*, 1995; *Barckhausen et al.*, 2001]. The location of the Nicoya peninsula, close to the subduction plate boundary and above the seismogenic portion of the plate interface, provides an excellent location for geodetic and seismic studies of shallow subduction zone processes [*Lundgren et al.*, 1999; *Newman et al.*, 2002; *DeShon et al.*, 2003, 2006; *Norabuena et al.*, 2004; *Protti et al.*, 2004; *Brown et al.*, 2009; *LaFemina et al.*, 2009; *Outerbridge et al.*, 2010; *Feng et al.*, 2010; *Walter et al.*, 2011].

[4] Several episodes of transient strain have been detected in the Nicoya Peninsula since 2000 from the analysis of several observation types, including GPS [*Protti et al.*, 2004; *Outerbridge et al.*, 2010], borehole pressure [*Davis and Villinger*, 2006; *Davis et al.*, 2011], seismicity [*Brown et al.*, 2009; *Walter et al.*, 2011] and fluid flow [*Brown et al.*, 2005; *Tryon*, 2009]. However, given the limited spatial and temporal coverage of sensors and data noise, it has not been possible to determine the recurrence interval for such events. In this paper, we re-analyze the GPS data of *Outerbridge et al.* [2010], add new data, and describe a new technique to identify slow slip events in GPS time series in the presence of noise. The new analysis allows us to define an average recurrence interval and investigate variations in event characteristics for slow slip events in the Nicoya region for the 2002–2011 time period.

2. GPS Data and Analysis Techniques

[5] The Nicoya continuous GPS network has been operating since 2002 [*Outerbridge et al.*, 2010]. By end of 2010, a total of 19 CGPS stations had been installed, although not all stations remained operational. Most of the stations were installed after 2006. *Outerbridge et al.* [2010] provide detailed site descriptions of the network. In our study, we use 12 stations that were installed on or before 2008 (Figure 1). We excluded stations with less than two years of observations because it is hard to get a robust estimate of inter-SSE rate and seasonal parameters with less than two years of observation. We analyzed all available GPS data from 2002 to 2011 using the GIPSY 6.1 software package, developed at the Jet Propulsion Laboratory (JPL), which includes an updated atmospheric model [*Boehm et al.*, 2006] and absolute satellite antenna phase center corrections [*Schmid et al.*, 2007]. Our processing strategy first generates daily point position solutions [*Zumberge et al.*, 1997; *Sella et al.*, 2002] for each station using the orbital parameters and satellite clock estimates from JPL. We adopt the single receiver phase ambiguity resolution algorithm [*Bertiger et al.*, 2010]

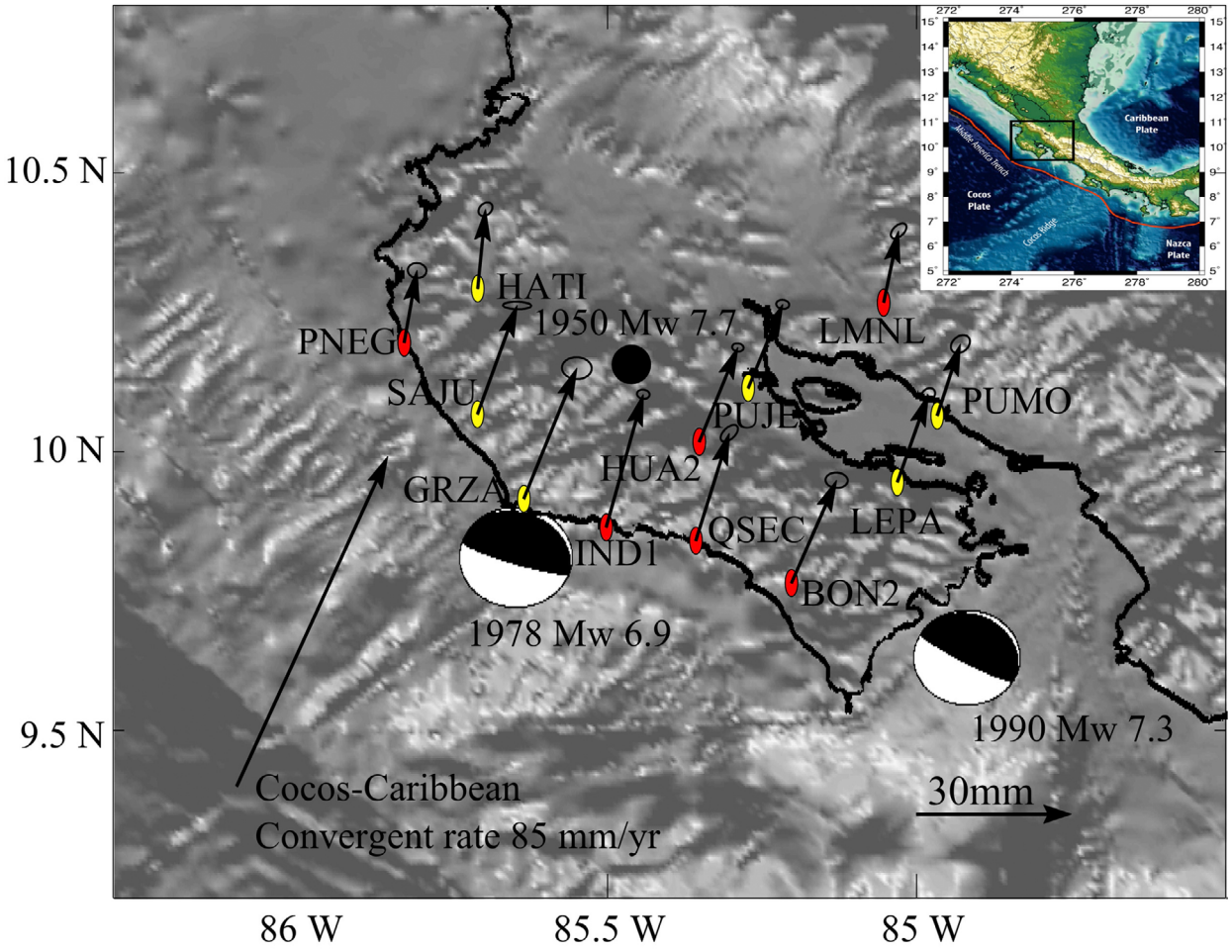

Figure 1. Shaded relief of Nicoya peninsula shows the locations of GPS stations and three recent large earthquakes (the 1950 earthquake is shown as a black circle). Red circles mark the CGPS stations used as reference stations in the data filtering process, yellow circles mark the remaining CGPS stations used in our study. The focal plane solutions were obtained from the Harvard CMT catalog. The approximate location of the 1990 earthquake is from *Protti et al.* [1995]. Station velocities are relative to a fixed Caribbean plate.

to solve integer ambiguities for each station. Bias-fixed daily solutions are then rotated into the ITRF2008 reference frame [*Altamimi et al.*, 2011]. The resulting raw daily GPS time series have average RMS scatters of 3 mm, 3 mm, and 8 mm in the north, east and vertical component, respectively (Figure 2 and auxiliary material).[1]

[6] Recognizing slow slip events in noisy position time series is challenging. GPS time series, especially in the tropics, may be affected by colored (time-correlated) noise [*Mao et al.*, 1999]. Colored noise probably reflects residual atmospheric, orbital effects or local site/ground effects, and may be difficult to distinguish from slow slip events. We have developed a time series analysis approach to solve this problem, which involves the following steps: (i) determining and removing a secular rate, (ii) visual detection of slow slip events over the whole network, (iii) fitting GPS time series with a customized model based on prior information from step 2, (iv) defining and removing Common Mode Error (CME), and (v) fitting the cleaned time series with a customized model to recover the SSE parameters.

3. Positionogram

[7] SSE detection requires spatial-temporal analysis of continuous GPS (CGPS) data acquired by dense

[1]Auxiliary materials are available in the HTML. doi:10.1029/2012GC004058.

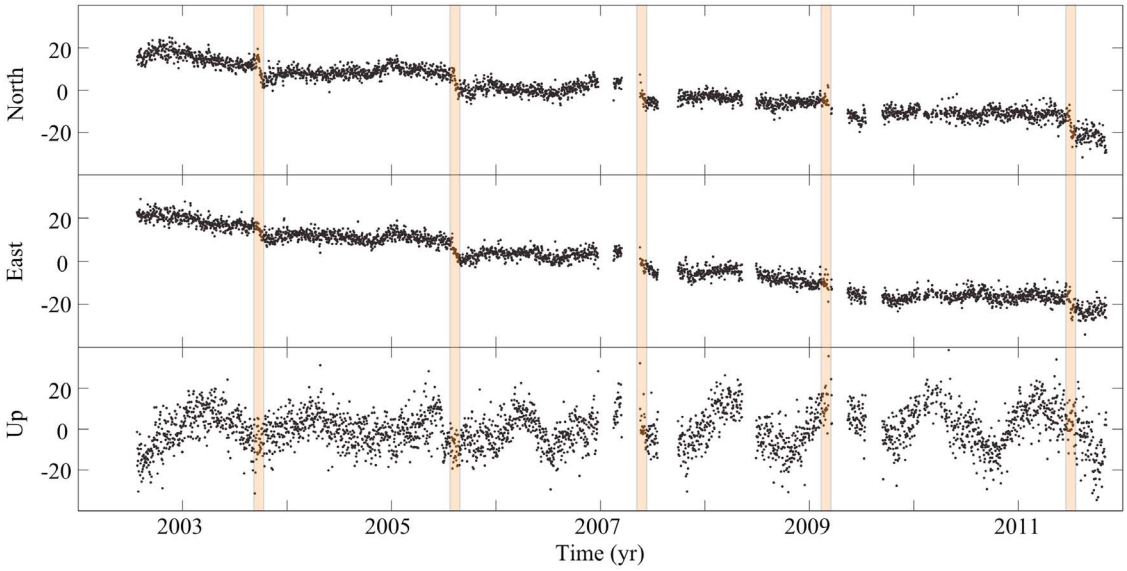

Figure 2. Raw GPS time series for station IND1 (Inter-SSE velocity removed). Each black dot represents daily position estimate. Five brown bars mark the occurrence of the SSEs in the time series. RMS scatters of the time series are 3 mm in both horizontal components and 8 mm in the vertical. Gaps in the time series are due to power outage or memory problems of the GPS receivers.

networks operating above subduction zones. Typically such information is displayed as a series of detrended time series, which works well when the SSE's offset is significantly higher than the background noise. However, the high noise level in the tropics can often mask SSEs, especially those with low or moderate offsets. In order to improve SSE detection in low signal-to-noise ratio environments, we developed a visual spatial-temporal detection technique, resulting in a display we term a positionogram [*Jiang and Wdowinski*, 2008]. A similar technique was introduced to study CGPS time series in the Basin and Range province of North America [*Wernicke and Davis*, 2010].

[8] The positionogram approach was inspired by wavelet analyses that use color to present quantitative information about relations between time and frequency domains. In the positionogram, colors

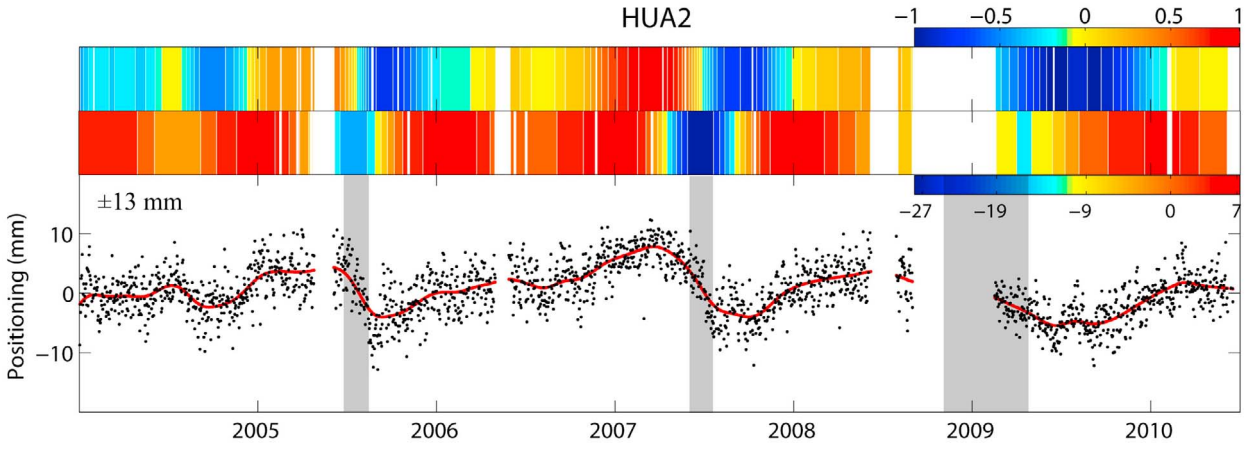

Figure 3. Graphical illustration of the transition from 2-D time-positioning representation of GPS time series to 1-D color bar representation. (bottom) GPS time series of the east component of station HUA2. The red line marks the spline fit to the data. The gray bars mark where slow slip events are determined based on the spatiotemporal analysis method (section 4). (middle) 1-D color presentation of the position-rate plot. Unit in mm/yr. (top) 1-D color plot of the position time series. Unitless, the scale of the upper color is normalized to the maximum site displacement (13 mm).

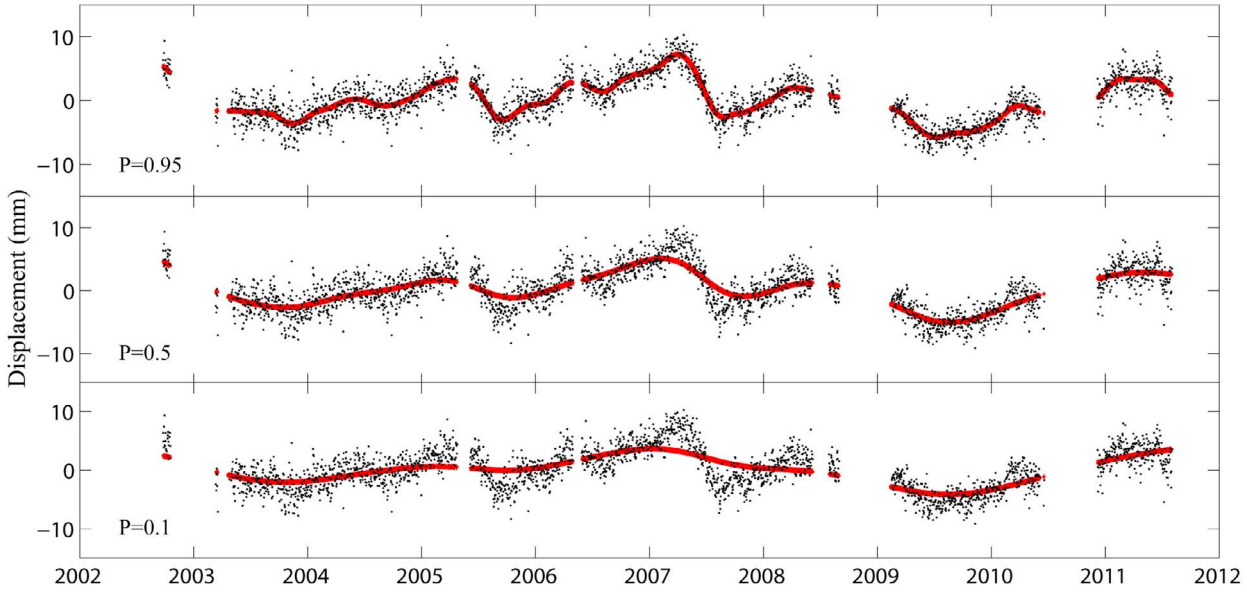

Figure 4. Sensitivity analysis of the smoothing parameter (P), which determines the cubic spline fit to the data. The fit level increases with increasing values of P. The analysis indicates that smoothing parameter P = 0.95 is most suitable for this study. The GPS data are of the east component of HUA2 series.

are used to represent displacement patterns in time and space. We first transform the standard detrended 2-D time series (one dimension is time and the other is position) into a 1-D color-coded presentation using a smoothing cubic spline fit to the time series. Then we normalize the spline by the minimum and maximum values and convert the normalized series to a 1-D color-coded plot. The spline is plotted one-dimensionally along the time axis using color to describe displacement changes (Figure 3).

[9] The smoothing cubic spline minimizes the function

$$W = P\chi^2 + (1-P)\int |S''(x)|^2 dx$$
$$= P\sum_i w_i(y_i - s(x_i))^2 + (1-P)\int \left(\frac{ds^2}{dx^2}\right)^2 dx$$

where χ^2 is the chi-square of the spline fit to the data, P is the smoothing parameter for the spline S. x_i, y_i and w_i are the time, displacements and formal errors of the GPS measurements. The first term on the right P χ^2 determines how well the spline fits the data. The second term is the second derivative of the spline, which quantifies the curvature of the spline. The smoothing spline is determined by balancing two contradictory criteria, goodness of fit and smoothness of curvature, where the tradeoff is set by the spline's smoothing parameter P, ranging from 0 to 1. Notice that putting $P = 0$ removes the constraint on χ^2 and the spline will have the smallest curvature which becomes a best fit straight line. On the other side, $P = 1$ results in a minimized χ^2 and forces the spline to exactly fit the data. In order to determine the most suitable smoothing parameter, we conducted a sensitivity study using various values of the smoothing parameter P. We chose a value ($P = 0.95$) that detects the SSE best and can also reflect the seasonal change in the time series (Figure 4).

[10] We apply the same procedure to all GPS time series and combine the 1-D color plots of each component into a single 2-D color plot according to the geographic location of the GPS sites. As indicated above, the time series are normalized to their respective maximum displacement in order to reduce station-varying seasonal amplitude effects in the network. The individual time series in the positionogram are therefore dimensionless, with amplitudes ranging from −1 to 1. The color plots, which are arranged according to the geographical distribution of the stations, incorporate the spatial information inherent in the network, thus providing 3-D information (time, space, and displacement) in color, facilitating visualization and easy detection of transient deformation. It is also easy to distinguish correlated and uncorrelated events, and to

Table 1. CGPS Locations and Inter-SSE Velocities

Station[a]	Latitude (deg)	Longitude (deg)	Vel08[b] (mm/yr)	VelCa[c] (mm/yr)	RMS (mm)	Annual (mm)	Semi-Annual (mm)
BON2	9.764	−85.203					
N			29.1 ± 0.56	22.1 ± 0.63	2.1	3.3	0.9
E			21.8 ± 0.43	8.8 ± 0.48	2.2	0.8	0.4
V			−7.5 ± 1.25		7.0	4.8	1.3
GRZA	9.915	−85.636					
N			34.9 ± 0.78	28.1 ± 0.84	2.1	1.8	0.5
E			23.3 ± 0.65	10.3 ± 0.69	1.9	1.5	0.4
V			−12.6 ± 0.54		7.1	4.9	0.5
HATI	10.291	−85.710					
N			23.9 ± 0.15	17.1 ± 0.34	1.5	1.2	0.7
E			14.3 ± 0.42	1.5 ± 0.47	1.5	0.5	0.6
V			−5.2 ± 0.43		5.1	6.5	1.0
HUA2	10.017	−85.352					
N			27.2 ± 0.14	20.3 ± 0.33	1.9	1.6	0.3
E			20.4 ± 0.12	7.5 ± 0.25	1.9	0.9	0.4
V			−6.3 ± 0.73		5.8	5.4	1.3
IND1	9.864	−85.585					
N			35.5 ± 0.21	28.6 ± 0.36	2.5	1.4	0.1
E			20.2 ± 0.19	7.2 ± 0.29	2.3	0.9	0.1
V			−12.1 ± 0.50		7.7	7.4	0.8
LEPA	9.945	−85.031					
N			25.8 ± 0.19	18.8 ± 0.35	1.3	1.8	0.4
E			19.0 ± 0.39	6.0 ± 0.45	1.5	0.8	0.4
V			−12.1 ± 1.01		5.2	4.6	1.8
LMNL	10.268	−85.053					
N			22.4 ± 0.12	15.4 ± 0.32	1.5	1.7	0.6
E			15.7 ± 0.52	2.9 ± 0.56	1.4	0.8	0.4
V			−3.5 ± 0.50		5.4	6.8	1.4
PNEG	10.195	−85.829					
N			22.3 ± 0.43	15.5 ± 0.53	2.1	1.9	0.2
E			15.3 ± 0.42	2.5 ± 0.47	2.0	1.2	0.3
V			−5.8 ± 1.34		7.1	6.9	2.9
PUJE	10.110	−85.270					
N			25.0 ± 0.23	18.0 ± 0.37	2.2	2.2	0.1
E			19.6 ± 0.18	6.7 ± 0.28	2.3	1.7	0.1
V			−4.7 ± 0.53		6.4	4.1	1.1
PUMO	10.064	−84.967					
N			22.5 ± 0.36	15.4 ± 0.46	1.9	2.0	0.3
E			17.4 ± 0.59	4.5 ± 0.63	1.9	0.7	0.4
V			−7.6 ± 0.48		6.4	5.1	1.3
QSEC	9.840	−85.357					
N			30.0 ± 0.17	23.1 ± 0.34	1.4	2.2	0.3
E			19.5 ± 0.59	6.5 ± 0.63	1.5	0.3	0.3
V			−7.1 ± 1.30		5.5	3.4	1.0
SAJU	10.067	−85.711					
N			30.2 ± 0.74	23.4 ± 0.80	2.2	1.5	0.2
E			20.6 ± 0.10	7.7 ± 0.23	2.1	0.6	0.8
V			−9.9 ± 0.25		7.4	6.6	0.5

[a]Stations are listed in alphabetical order. All station coordinates are in ITRF 2008 reference frame.
[b]North, east, and vertical inter-SSE velocities in ITRF2008 reference frame. Inter-SSE velocity uncertainties are from noise analysis results (Table 3, flt).
[c]Horizontal velocities are referred to a stable Caribbean plate (C. DeMets, personal communication, 2011).

find anomalous stations, e.g., those affected by unstable monuments or local sources such as volcanic deformation.

[11] Due to the nature of slow slip events (movements that are the reverse of the subducting plate motion direction over short time spans), we identify slow slip events as areas in the positionogram that have high negative gradients. In our color scheme, these are yellow/green bands in the transition region from red to blue. A separate but similar technique, which focuses on the position-rate

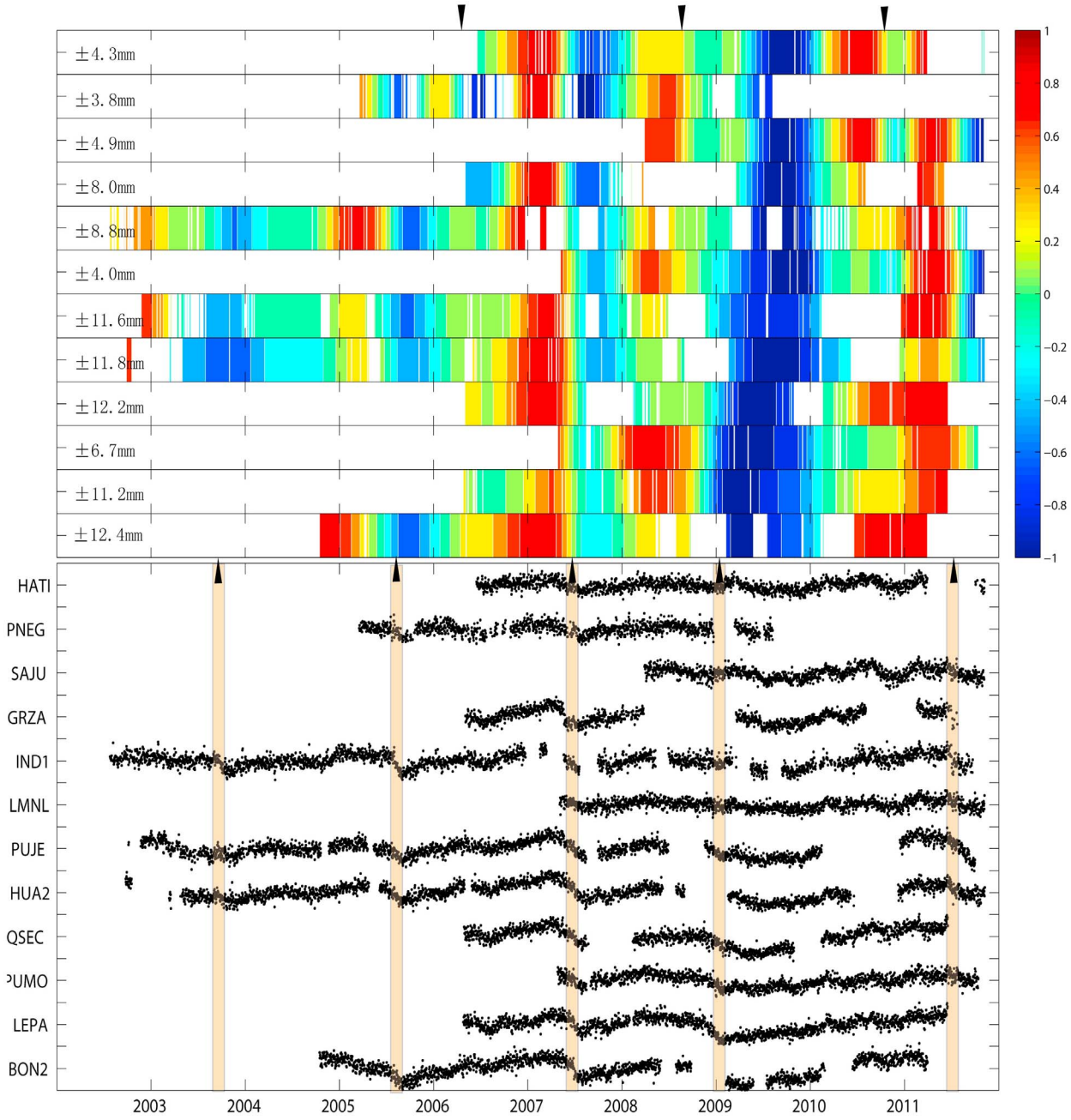

Figure 5. (bottom) East component of the raw GPS observations. The brown bars are time and duration information we observed from the positionogram. Additional time series are in the auxiliary material. (top) Positionogram for the east component of the Costa Rica CGPS network. Slow slip events occur at the transition from red to blue. Stations are arranged based on their locations from northwest (top) to southeast (bottom). Each row in the positionogram is normalized by its maximum amplitude, which is listed in the left side of each row. Black arrows at the base of the positionogram show the timing of the network-wide SSEs. The arrows at the top of the positionogram point to the three small SSEs observed in northern peninsula.

change, is also introduced (Figure 3). In the positioning-rate-gram, colors are used to represent rate changes in time and space. We calculate the derivatives of the spline in the time domain and plot one-dimensionally along the time axis to describe rate changes. In the positioning-rate-gram, the SSEs are regions of large negative rates, which are the blue areas. Because the positioning-rate-gram

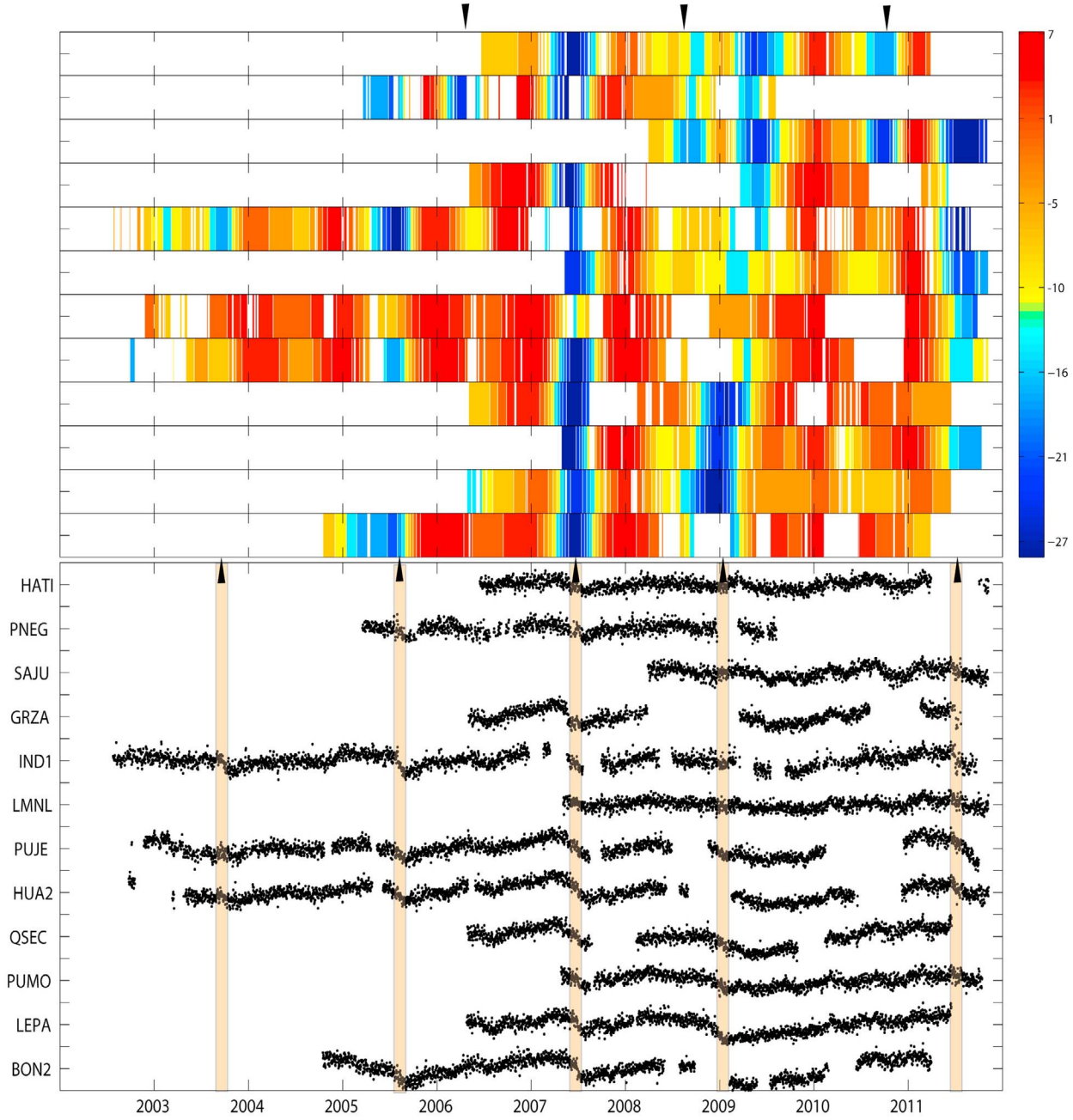

Figure 6. (bottom) East component of the raw GPS observations. (top) Positioning-rate-gram for the east component of the Costa Rica CGPS network. Slow slip events marked in blue. Stations are arranged in the same order as in Figure 5.

marks the SSEs with one color instead of color gradients, it makes the plot straightforward for interpretation.

[12] Seasonal signals exhibit similar characteristics, but also differ from slow slip events in several important aspects. First, seasonal signals have longer duration, usually several months or longer. Second, one important class of seasonal signal, the annual term, by definition has a period of one year which can be modeled and removed. Third, seasonal signals are not likely to have a prominent east component of motion as observed by our CGPS stations (Table 1), which is typical of slow slip events in the Nicoya peninsula.

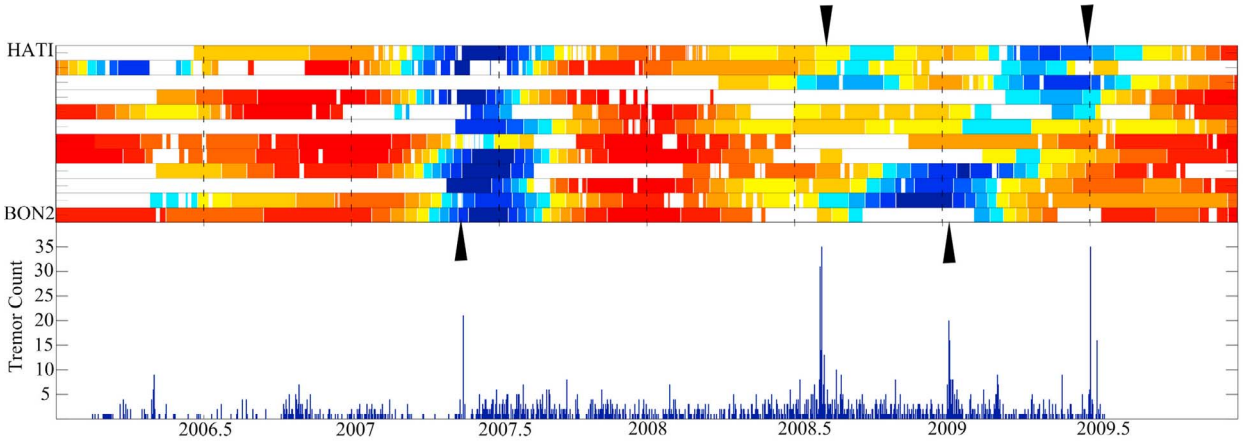

Figure 7. Comparison of (top) positioning-rate-gram and (bottom) tremor activity in Nicoya Peninsula. Arrows in the positioning-rate-gram mark the large SSEs in 2007.4 and 2009.0 (bottom) and smaller SSEs in 2008.6 and 2009.4 (top). Tremor data are from *Walter et al.* [2011]. Timing of the two large SSEs coincides with tremor activities in 2007 and 2009.0. The two tremor episodes in 2008.6 and 2009.4 coincide only with the northwest GPS stations.

These characteristics enable us to separate slow slip events from a variety of seasonal signals.

[13] We applied our method to data from the Costa Rica CGPS network. The east-west component experienced larger slip during the 2007 slow slip event [*Outerbridge et al.*, 2010], and has relatively smaller seasonal effects compared to the other two components (Table 1). Thus we choose the E-W component to detect slow slip events using the positionogram approach. We compute the positioning-rate-gram as well and plot it separately. The results (Figures 5 and 6) indicate that five distinct SSEs occurred during 2002–2011, with event middle times in 2003, 2005, 2007, 2009 and 2011. In 2006, 2008 and 2010, three stations show SSE-like patterns. However, the displacements are small and only affect a few stations in the northern peninsula (top of the positionogram), thus are not counted when calculating the recurrence interval for the whole area. The 2011 event is ongoing and needs more data in order to obtain a robust solution. Nevertheless the strong red stripe at the end of the positionogram clearly indicates the occurrence of this new event. By inspecting the positionogram, we estimated the approximate time, duration and recurrence interval for SSEs in the area and used theses parameters as a priori information to the parameter estimation. Figure 7 also shows that the May 2007 event migrated from NW to SE, parallel to the trench. The 2009 event, which has a different migration direction, started in the SE then propagated to NW over a period of ~180 days. The observed migration of SSE agrees well in space and time with seismic tremor detected in the same area [*Schwartz et al.*, 2011].

4. Parameter Estimation

[14] We then conducted a parameter estimation analysis in order to rigorously separate transient deformation signals from secular plate motion, seasonal effects, and site-specific noise sources. In our approach, a site-specific model is developed to fit the raw position estimates, with estimates from the positionogram used as a priori inputs to the model for event time and duration. The residual time series are then used to estimate Common Mode Error (CME) in the GPS network. The resulting cleaned time series are then used to obtain final parameter estimation (Tables 1 and 2).

[15] The site-specific model fits the daily GPS coordinates, accounting for the effects of slow slip events and some fraction of time-correlated noise, namely noise with annual or semi-annual periodicities:

$$x(t_i) = a + bt_i + c\sin(2\pi t_i) + d\cos(2\pi t_i) + e\sin(4\pi t_i) + f\cos(4\pi t_i) + \sum_{j=1}^{m} g_j H(t_i - t_j) + \sum_{k=1}^{n} \frac{U_k}{2}\left(\tanh\frac{t_i - T_k}{\tau_k} - 1\right) + v_i$$

where $x(t_i)$ is the position of a GPS station at the observation epoch t_i, relative to the starting epoch

Table 2. Best Estimation of Start Date, Duration, and Slip of the Detected SSEs

Station	Start[a] (doy)	Duration (days)	North[b] (mm)	East[b] (mm)	Vertical[b] (mm)
BON2					
2005	198	30	−9.5 ± 1.1	−10.9 ± 1.2	2.3 ± 3.5
2007	163	30	−11.5 ± 1.1	−11.5 ± 1.1	4.9 ± 3.7
2009	−80	180	−10.0 ± 1.4	−14.4 ± 1.4	11.7 ± 4.4
GRZA					
2007	140	33	−5.7 ± 1.3	−5.2 ± 1.1	−1.3 ± 4.5
2009	−80	180	−9.3 ± 1.9	−6.8 ± 1.8	4.4 ± 7.1
2011	170	20	−9.5 ± 2.7	−5.1 ± 2.5	−0.8 ± 10.1
HATI					
2007	137	26	−2.2 ± 0.7	−3.8 ± 1.8	3.4 ± 2.9
2008	210	20	−2.6 ± 0.8	−1.3 ± 2.1	2.3 ± 3.2
2009	150	30	−0.2 ± 0.7	−2.6 ± 1.6	2.2 ± 2.8
2010	275	30	−2.0 ± 1.0	−1.5 ± 2.6	1.2 ± 4.2
HUA2					
2003	254	30	−3.2 ± 0.4	−4.7 ± 0.4	−2.7 ± 1.3
2005	198	30	−3.9 ± 0.4	−5.8 ± 0.4	1.7 ± 1.2
2007	160	27	−3.1 ± 0.3	−8.7 ± 0.4	8.1 ± 1.2
2009	−80	180	−3.4 ± 0.4	−10.8 ± 0.5	8.5 ± 1.6
2011	170	20	−4.6 ± 0.5	−4.5 ± 0.6	1.5 ± 1.9
IND1					
2003	254	30	−7.5 ± 0.4	−6.5 ± 0.4	−1.4 ± 1.2
2005	198	30	−8.3 ± 0.5	−6.6 ± 0.4	0.4 ± 1.4
2007	152	30	−6.0 ± 0.6	−7.0 ± 0.7	1.5 ± 2.0
2009	−80	180	−7.8 ± 0.6	−8.7 ± 0.6	2.5 ± 1.8
2011	170	20	−10.4 ± 0.8	−5.0 ± 0.7	−4.0 ± 2.6
LEPA					
2007	165	30	−7.1 ± 1.3	−6.3 ± 1.8	19.3 ± 4.5
2009	−80	180	−8.1 ± 1.7	−12.6 ± 2.4	22.3 ± 6.0
LMNL					
2007	168	24	−2.6 ± 0.5	−2.9 ± 1.2	4.1 ± 2.8
2009	−80	180	−2.5 ± 0.4	−5.3 ± 1.5	7.2 ± 2.9
2011	170	20	−2.4 ± 0.4	−3.0 ± 1.3	−1.8 ± 2.7
PNEG					
2005	198	30	−4.2 ± 0.9	−3.0 ± 1.1	−0.2 ± 3.8
2007	135	25	−1.7 ± 1.0	−3.1 ± 1.2	−1.0 ± 4.0
2009	−80	180	−5.8 ± 1.2	−2.8 ± 1.5	3.6 ± 6.1
PUJE					
2003	254	30	−2.6 ± 0.6	−5.5 ± 0.6	−2.6 ± 1.8
2005	198	30	−2.8 ± 0.7	−5.7 ± 0.8	3.3 ± 2.0
2007	159	28	−1.2 ± 0.6	−7.2 ± 0.7	6.0 ± 2.0
2009	−80	180	1.6 ± 1.0	−8.3 ± 1.2	1.9 ± 3.5
2011	170	20	−0.7 ± 1.4	−4.4 ± 1.5	2.5 ± 4.2
PUMO					
2007	165	24	−3.2 ± 1.0	−3.6 ± 1.5	11.4 ± 4.5
2009	−80	180	−3.2 ± 0.9	−8.9 ± 1.3	15.8 ± 3.7
2011	170	20	−1.4 ± 1.0	−2.2 ± 1.5	−1.4 ± 5.1
QSEC					
2007	160	30	−4.5 ± 0.5	−11.2 ± 1.6	4.2 ± 2.7
2009	−80	180	−7.2 ± 0.7	−12.5 ± 2.2	3.4 ± 3.1
SAJU					
2008	210	20	−6.1 ± 1.0	−2.9 ± 0.9	2.7 ± 4.1
2009	150	30	−4.5 ± 1.0	−4.8 ± 1.0	2.5 ± 4.8
2010	275	30	−3.9 ± 1.1	−2.0 ± 1.2	2.1 ± 5.0
2011	170	20	−6.9 ± 1.0	−4.1 ± 1.1	−2.4 ± 4.9

[a]Start date and duration of each SSE. For 2007 SSE, the start day and duration are estimated. The 2003, 2005, 2009 and 2011 SSE start time and duration are fixed due to data limit. Station SAJU and HATI are estimated using different event times and durations.
[b]North, east, and vertical SSE displacement at each GPS station, errors are scaled to fit the velocity uncertainty estimates in Table 3.

of time series. The first two terms are the intercept a and secular rate b. c, d, e and f are the phases and amplitudes of the annual and semi-annual variations, g_j is an offset caused by GPS hardware replacement, station relocation, or unknown sources. $H(t_j)$ is the Heaviside function on the offset onset time. The parameters U, T and τ are the event offset, the midpoint time of the modeled transient event, and the duration half width respectively, following the formulation of *Larson et al.* [2004]. v_i is the data residual noise. The last large earthquake in this region occurred in 1990 (Mw = 7.0) [*Protti et al.*, 1995]. *Norabuena et al.* [2004] studied the post-seismic relaxation process in this area and their results showed negligible impacts in GPS time series caused by post-seismic deformation. An Mw 6.1 strike slip earthquake occurred close to the GPS network in January, 2009. We calculated the co-seismic displacement caused by the earthquake using an elastic dislocation model [*Okada*, 1985]. The largest surface displacement in our network due to the earthquake is less than 1 mm, suggesting that the earthquake effect is negligible. Our characterization method is similar to the method of *Outerbridge et al.* [2010], with additional terms accounting for annual and seasonal variations.

[16] The transient components are only applied to the time periods defined by the positionogram (Figures 5 and 6). During these periods, the wavelength of the slow slip signal is significantly shorter than that of the seasonal signal in 4 out of 5 events. Hence the slow slip events in the four cases can be determined precisely. However, the 2009 event lasts about half a year, similar to the seasonal signal, hence estimation of the transient event is affected by the seasonal term, especially by the vertical component. The inter-SSE velocity for each station is estimated using observations that are free of transient events. Slow slip event duration and middle time are estimated using grid search for the 2007 event. Duration and middle time for the other SSEs are fixed and all other parameters including seasonal signals, secular rates and SSE slips are estimated using least square methods. Stations SAJU and HATI at the top of the positionogram differ from other stations in terms of SSE time and duration. Instead of fitting a long-term SSE centered in 2009, we estimated two separate short-term SSEs with mid-times on 2008.6 and 2009.4; the results agree well with tremor activities reported by *Walter et al.* [2011].

[17] Several regional GPS network filtering techniques have been developed to improve the signal/noise ratio in GPS time series. In our study, we adopted the approach suggested by *Wdowinski et al.* [1997], stacking a set of fiducial GPS sites in the Nicoya CGPS network (Figure 1) and computing the weighted mean of the daily position residual time series (CME). The time series are termed CME and are then subtracted from all the stations to obtain the cleaned time series. We require a minimum of three observations at each epoch to calculate the CME. After this removal, typical RMS scatters for the time series are 2 mm (north), 2 mm (east) and 6 mm (vertical), significantly improved with respect to the original raw time series, and similar to values obtained for stations in the drier western US. Sample GPS time series and model fits are shown in Figure 8.

[18] To quantify the noise level in our CGPS time series, we calculated the noise amplitude by applying the Allan Variance of the Rate (AVR) to the time series [*Hackl et al.*, 2011]. The AVR has been fit with an error model accounting for white noise, flicker noise, random walk and an annual signal:

$$\sigma_v^2 = a_{wn}\tau^{-3} + a_{fl}\tau^{-2} + a_{rw}\tau^{-1} + \frac{36T^2a_{an}^2}{\pi^2\tau^4}\left(\frac{T}{\pi\tau}\sin\left(\frac{\pi\tau}{T}\right) - \cos\left(\frac{\pi\tau}{T}\right)\right)^2$$

where σ_v is the velocity uncertainty, a_{wn}, a_{fl} and a_{rw} are the coefficients for white, flicker and random walk respectively, and a_{an} is the annual signal amplitude. τ is the AVR sampling interval and T is the period of the signal, here T = 365 days. *Zhang et al.* [1997] derived analytic expressions for weighted linear regressions to quantify the effective stochastic models of the white noise and random walk. In the case of white noise, the rate variance can be expressed by [see *Zhang et al.*, 1997, equation (1) and Appendix (A23)]:

$$(\sigma_r^2)_{WN} \cong \frac{12b_{wn}^2}{NT^2} \quad (1)$$

where b_{wn} is the amplitude of the white noise, N is the number of points in the time series, and T is the total observation span. For the rate variance caused by random walk *Zhang et al.* [1997] found [see *Zhang et al.*, 1997, equation (2) and Appendix (A30)]:

$$(\sigma_r^2)_{RW} = \frac{b_{rw}^2}{T} \quad (2)$$

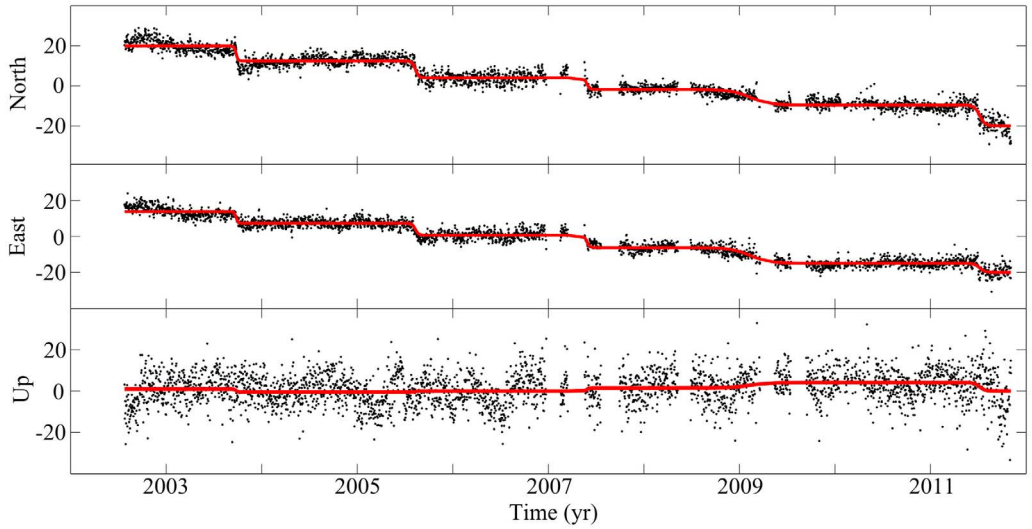

Figure 8. Time series and best fit model of station IND1 from 2002 to 2011. Inter-SSE velocities, seasonal signals and antenna change offsets have been removed from the time series. Time series show five distinct SSEs. The 2009 event has a significantly longer duration compared to the other four events.

where b_{rw} is the amplitude of random walk. *Williams* [2003] found the same relations for white noise [*Williams*, 2003, equation (21)] and random walk [*Williams*, 2003, equation (22)]. Additionally, they found the following expression for the rate variance in the case of flicker noise [*Williams*, 2003, equation (24)]:

$$(\sigma_r^2)_{FL} \cong \frac{9b_{fl}^2}{16\Delta T^2(N^2-1)} \tag{3}$$

where b_{fl} is the amplitude of flicker noise, ΔT is the sampling interval and N is the number of points. Therefore, for daily solution time series without gaps equation (3) can be approximated by:

$$(\sigma_r^2)_{FL} \cong \frac{9b_{fl}^2}{16T^2} \tag{4}$$

On the other hand, *Williams* [2003, equation (25)], *Bos et al.* [2008, equation (29)], and *Hackl et al.* [2011, equation (4)] showed that the rate variance of time series affected by colored noise can be expressed by:

$$\sigma_{WN}^2 \cong \frac{a_{wn}}{T^3} \tag{5}$$

$$\sigma_{FL}^2 \cong \frac{a_{fl}}{T^2} \tag{6}$$

$$\sigma_{RW}^2 \cong \frac{a_{rw}}{T} \tag{7}$$

for white noise, flicker noise, and random walk, respectively. Combining equations (1), (2), and (4) with (5), (6), and (7), respectively, leads to:

$$b_{wn} \cong \sqrt{\frac{a_{wn}}{12}}$$

$$b_{fl} \cong \frac{4}{3}\sqrt{a_{fl}}$$

$$b_{rw} \cong \sqrt{a_{rw}}$$

We calculated amplitudes of white noise, flicker noise and random walk for the raw time series (raw), time series after SSE removed (sse), and time series with both SSE and CME are removed (flt). The results are shown in Table 3. The average noise amplitude after SSE and CME are removed is 2.8 mm for horizontal components and 9 mm for the vertical component. Our results also suggest SSE in the time series appears as random walk noise, thus the true random walk noise values are small after removing the SSE. The white plus colored noise amplitude is 2–6 times smaller than the SSE horizontal surface displacement listed in Tables 1 and 2, suggesting that our SSE parameter estimates are robust. We use the filtered (flt) values to estimate our uncertainty values for the inter-SSE velocity and other parameters in Tables 1 and 2.

5. Results

[19] Our new SSE detection approach successfully identified multiple slow slip events and defined

Table 3. Noise Characterizations of the CGPS Time Series According to a White, Flicker, and Random Walk Noise Model

Site	b_{wn}[a]			b_{fl}[b]			b_{rw}[c]			σ (v)[d]		
	raw	sse	flt	raw	sse	flt	raw	sse	flt	raw	sse	flt
BON2												
North	1.89	1.78	1.45	2.29	2.90	1.48	0.32	0.04	0.07	2.43	0.44	0.56
East	2.00	1.58	1.39	0.69	2.92	1.32	0.37	0.01	0.05	2.78	0.35	0.43
Up	6.16	6.21	5.62	6.92	6.93	3.57	0.27	0.00	0.16	2.20	0.81	1.25
GRZA												
North	1.91	1.97	1.51	2.63	2.63	1.26	0.32	0.09	0.09	2.68	0.83	0.78
East	1.79	1.48	1.35	0.00	2.42	0.75	0.42	0.12	0.08	3.46	1.05	0.65
Up	6.43	6.30	5.49	7.13	7.95	3.66	0.60	0.00	0.00	5.14	1.14	0.54
HATI												
North	1.85	1.92	1.94	2.38	2.26	0.94	0.10	0.00	0.00	0.91	0.34	0.15
East	1.66	1.69	1.77	2.24	2.19	0.60	0.11	0.00	0.05	0.99	0.32	0.42
Up	5.75	5.69	6.29	5.60	5.88	2.68	0.22	0.00	0.00	2.09	0.87	0.43
HUA2												
North	1.55	1.60	1.54	2.99	2.88	1.58	0.00	0.00	0.00	0.25	0.24	0.14
East	1.73	1.63	1.45	2.17	2.54	1.40	0.22	0.00	0.00	1.43	0.22	0.12
Up	5.53	5.61	5.47	6.33	6.22	3.04	0.24	0.09	0.11	1.63	0.80	0.73
IND1												
North	1.93	2.13	1.66	3.75	3.50	2.45	0.14	0.00	0.00	0.95	0.29	0.21
East	1.98	2.00	1.55	3.16	3.18	2.31	0.14	0.00	0.00	0.90	0.26	0.19
Up	6.87	6.68	5.80	7.79	8.78	5.97	0.00	0.00	0.00	0.67	0.73	0.50
LEPA												
North	1.74	1.61	1.49	1.39	2.13	0.94	0.24	0.00	0.01	2.07	0.31	0.19
East	1.89	1.63	1.63	0.00	2.33	0.80	0.37	0.00	0.04	3.12	0.34	0.39
Up	5.65	5.04	5.80	4.73	7.57	3.89	0.75	0.00	0.10	6.38	1.11	1.01
LMNL												
North	1.85	1.87	1.44	2.08	2.04	0.60	0.07	0.00	0.00	0.75	0.36	0.12
East	1.61	1.66	1.38	2.10	1.99	0.00	0.11	0.00	0.06	1.05	0.35	0.52
Up	6.00	6.12	5.65	7.32	7.04	2.68	0.00	0.00	0.00	1.35	1.25	0.50
PNEG												
North	2.16	2.26	2.19	3.54	3.38	2.52	0.00	0.00	0.00	0.61	0.58	0.43
East	2.19	2.24	2.17	3.09	2.95	2.45	0.00	0.00	0.00	0.53	0.51	0.42
Up	7.62	7.91	8.91	9.39	9.39	7.79	0.00	0.00	0.00	1.75	1.61	1.34
PUJE												
North	1.74	1.82	2.04	3.02	2.99	2.70	0.05	0.00	0.00	0.40	0.26	0.23
East	1.94	1.88	2.12	2.26	2.65	2.12	0.20	0.00	0.00	1.30	0.23	0.18
Up	6.03	6.06	6.96	6.54	6.77	6.17	0.11	0.00	0.00	0.92	0.58	0.53
PUMO												
North	1.65	1.64	1.51	2.04	2.15	0.00	0.14	0.00	0.04	1.35	0.39	0.36
East	1.66	1.51	1.40	1.37	2.15	0.00	0.25	0.00	0.06	2.40	0.39	0.59
Up	5.55	5.25	5.21	3.86	5.72	2.58	0.60	0.00	0.00	5.69	1.04	0.48
QSEC												
North	1.82	1.64	1.33	2.24	2.88	1.17	0.25	0.00	0.00	2.17	0.42	0.17
East	2.01	1.68	1.44	0.00	2.63	1.16	0.38	0.08	0.07	3.23	0.75	0.59
Up	6.45	6.36	5.51	5.76	6.35	1.17	0.23	0.00	0.15	2.09	0.94	1.30
SAJU												
North	1.64	1.73	2.19	2.77	2.65	0.00	0.24	0.00	0.07	2.59	0.60	0.74
East	1.71	1.74	2.11	2.06	2.13	0.00	0.21	0.00	0.00	2.21	0.48	0.07
Up	7.08	7.14	8.24	7.09	7.02	0.00	0.00	0.00	0.00	1.64	1.59	0.25

[a] b_{wn}: White noise amplitude; unit - mm·day$^{0.5}$; raw: raw time series results; sse: SSE removed time series results; flt: SSE and CME removed results.
[b] b_{fl}: Flicker noise amplitude, unit - mm.
[c] b_{rw}: Random walk amplitude; unit - mm·day$^{-0.5}$.
[d] σ (v): Velocity uncertainty of the time series; unit - mm·yr^{-1}.

their recurrence interval in the presence of noise (Figures 5 and 6). The cleaned time series suggests a SSE recurrence interval of 21 ± 6 months in this area. In addition, our approach can also detect event migration in space and time, as discussed below for individual events and illustrated in Figures 7 and 9. The key parameters characterizing the various SSEs are listed in Table 2, and are described below.

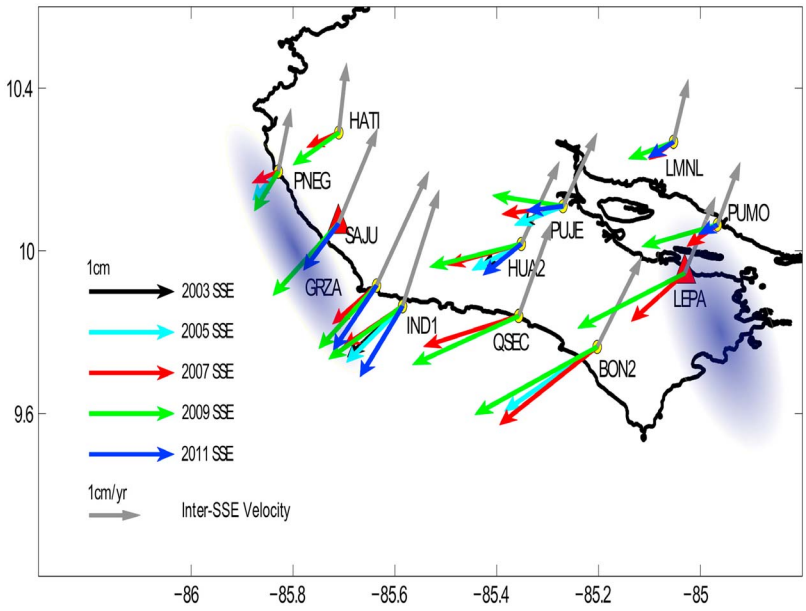

Figure 9. SSE slip distributions for each of the five events. The gray arrows are station inter-SSE velocities in a fixed Caribbean frame. The two blue areas are maximum slip patches of the 2007 event [*Outerbridge et al.*, 2010].

5.1. August 2003

[20] During this event, only three stations (IND1, HUA2, and PUJE) were operating [*Protti et al.*, 2004]. The displacement decreased from coastal station IND1 to the inland station PUJE, and lasted about 30 days. The transient displacements were nearly opposite to the direction of plate convergence (Figure 9). Two anomalous pressure transients were recorded offshore by borehole hydrological observations on May and October. The October event is one month after the CGPS-defined event time [*Davis and Villinger*, 2006].

5.2. July 2005

[21] This event was recorded by five stations (PNEG, IND1, BON2, HUA2, and PUJE). It had transient displacements similar to the 2003 event in both direction and magnitude. No other evidence indicating transient deformation was observed during this time.

5.3. May 2007

[22] This event was described by *Outerbridge et al.* [2010]. It was detected by all operating stations (eleven). Maximum surface displacement (~16 mm) was recorded at stations QSEC and BON2. The improved station spatial coverage allowed us to shed some light on transient event propagation direction and duration. Slip nucleated near the northern stations (PNEG, HATI), then propagated southward over a 30 day period. 52 seismic tremor episodes and a total of 232 low frequency earthquakes were detected in the area [*Brown et al.*, 2009], and coincided with timing of the SSE (Figure 7). By inverting surface motion data for the May 2007 event, *Outerbridge et al.* [2010] proposed a separation of slow slip into an updip northern patch and a downdip southern patch, which may be related to different properties of subducted crust beneath each patch. Our new GPS results suggest that the SSE may have initiated at the shallower northern patch defined by *Outerbridge et al.* [2010] and then propagated along-strike to the southeast.

5.4. January 2009

[23] Unfortunately five stations were offline during part of this event. Despite this, the event was recorded in sufficient detail to allow determination of a distinctive time evolution compared to earlier events (Figure 7). The event started in October 2008 and lasted for a half year, significantly longer than the earlier events. Southern stations in the network exhibit the largest surface displacements, with maximum amplitude ~17.5 mm within half a year (BON2). A cluster of tremor events was recorded during the same time period [*Walter et al.*, 2011]. Two stations in the north (SAJU and HATI) observed two separate short-term SSEs in 2008.6 and 2009.4. Comparisons of SSE in northern and southern stations show two distinct temporal types of slip (Figure 9). The southern stations (e.g.,

LEPA) show one long-term (~6 month) SSE, producing ~15 mm of surface displacement. In contrast, the northern stations (e.g., SAJU) observed two separate short-term (~1 month) SSEs with interval of approximately one year, with each SSE producing ~5 mm of surface displacement. In addition, on 2010.8, we observe a third SSE in the time series of SAJU, which is not apparent in the LEPA time series.

5.5. June 2011

[24] The event was observed by seven stations (most of the data had not yet been downloaded from the network at the time of our analysis). Our results show that stations IND1 and GRZA experienced significant SSE displacement during the event (Figure 8). The event starts in mid-June and lasts for ~20 days. The slip amplitudes and directions are very similar to the 2003 and 2005 events.

6. Discussion

[25] Noise analysis indicates that our technique significantly improves the signal-to-noise ratio for SSE parameters compared to the raw time series, and corresponding reduction of velocity uncertainties by 3–10 times. Previous studies [*Mao et al.*, 1999; *Hill et al.*, 2009; *King and Williams*, 2009] suggest a white plus flicker noise model describes the noise content for most GPS time series. However, our raw data exhibit high levels of random walk. This reflects the influence of SSE. For one day's observation, typical horizontal "noise" amplitude in the raw time series from white, flicker and random walk processes are 1.8 mm, 2.1 mm and 0.3 mm, versus 1.5 mm, 1.3 mm and 0.05 mm for the filtered solutions (flt time series). With an average of 6 years' continuous observation (~2000 days), white noise contribution to the position uncertainty is small (~0.03 mm) since it decreases with number of observations ($1/\sqrt{(N)}$). Removal of the SSE effects (sse, Table 3) does not reduce the white noise amplitude, but regional filtering (flt, Table 3) reduces the amplitude by ~10–20%. The reduction of flicker noise also results from removal of CME (flt, Table 3). The dominant colored noise in daily solutions is flicker noise and its amplitude is time independent. Although random walk noise is small in daily solutions, it increases with the number of daily observations ($\sqrt{(N)}$) and become the main contributor to the position uncertainty after 6 years (~13 mm for the raw). Since most of the random walk process is in fact SSE, the true noise is rather small. By removing SSE, we obtain 2.3 mm random walk noise for 6 years' observation. Note that noise contributions that could not be solved for in the accessible range of frequencies are set to zero. Applying a filter reduces the amplitude of white noise and especially flicker noise. As a consequence, the crossover period between flicker and random walk noise is shifted toward shorter periods and the amplitude for random walk can be obtained, which is not possible in the case of the unfiltered time series.

[26] A linear relation between SSE duration and event moment magnitude has been proposed using data from Cascadia [*Aguiar et al.*, 2009]. Using seismic and geodetic data, *Obara* [2010] found that slow slip source regions in southwest Japan are segmented, such that each segment has its own recurrence interval and migration direction. He also found that slow slip moment magnitudes from inversion of geodetic data are proportional to their recurrence intervals. If the same time-magnitude relation holds for Nicoya, the long recurrence interval and larger magnitude in the Nicoya peninsula may reflect differences in subduction rate or frictional conditions compared with Cascadia and Southwest Japan. In Nicoya, the subducting plate is younger and hotter compared to these other well-studied regions. These characteristics may influence frictional conditions, such that SSE events in Nicoya require a longer time to "load," but subsequently release a larger seismic moment. The moment magnitude from inversion of both campaign and continuous GPS data of the five significant SSEs in Costa Rica are between M_w 6.6 to M_w7.2 [*Outerbridge et al.*, 2010; *Jiang et al.*, 2011] larger than the GPS detected Cascadia SSE events (Mw 6.2–Mw 6.8) [*Szeliga et al.*, 2008] and short-term SSE in Japan [*Obara*, 2010]. Another possibility that potentially contributes to the apparently long recurrence interval here could be due to the fact that our GPS observations are not sensitive to small SSE. If these occasionally occur but remain undetected, we would overestimate the recurrence interval. Three small SSEs were detected at stations SAJU and HATI. If these events are included in the analysis, an average recurrence interval of ~1 year is obtained. Figure 6 shows that the northern stations (top) have a different SSE recurrence interval of ~one year during the observation period which differs from stations in the south. Hence it is possible that the plate interface in Nicoya is segmented, and has different slip distributions, magnitudes, and recurrence intervals of SSEs; in that case, a single

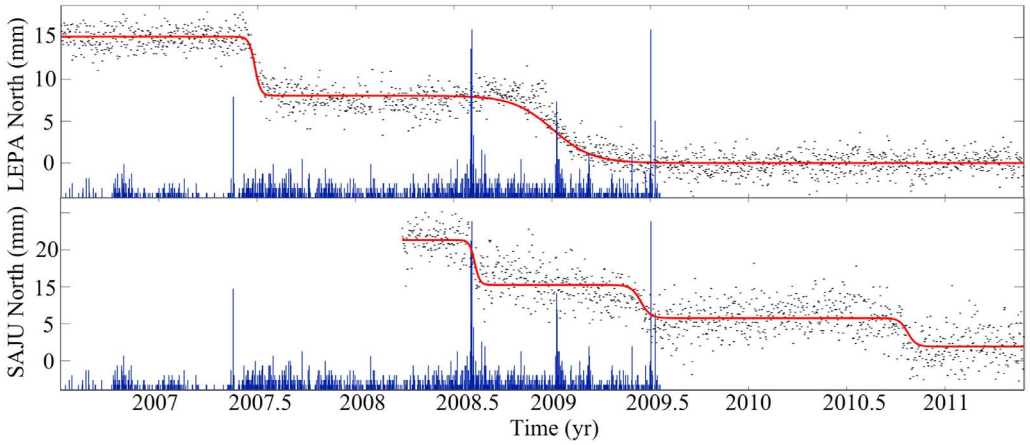

Figure 10. (top) North component of station LEPA focusing on the period 2006.5–2011 with seasonal signals and secular rates removed, leaving only the slow slip signal. The red line is the best fit model to the GPS time series. Blue bars represent a tremor histogram (same as Figure 7). (bottom) North component of station SAJU with tremor histogram in the background.

recurrence interval for the region may not be a useful description. Many SSEs in southwest Japan are detected by tiltmeters, which are much more sensitive to small changes compared to our GPS solutions. Similarly sensitive instrumentation and offshore observations may be required in Nicoya to resolve this issue.

[27] The 2009 event differed significantly from the others in both duration and magnitude. *Walter et al.* [2011] observed persistent seismic tremor from August 2008 to June 2009; their data show three peaks in tremor activity, referred to here as 2008.6, 2009.0 and 2009.5 (Figure 10). *Davis et al.* [2011] reported an August 16, 2008 event using borehole strainmeter measurements. This event coincides with the 2008.6 tremor activity with only 1–2 week latency. However, we do not detect these sub-events in all the GPS time series. The southern and northern GPS stations exhibit different behavior. While southern stations observed only one long-term SSE centered in 2009, northern stations observed two separate SSEs. It is possible that the associated surface displacements for the two sub-events are quite small, below the detection threshold for the southern stations. With current analytical techniques, GPS stations are only capable of detecting SSEs ≥ Mw 6 [*Peng and Gomberg*, 2010]. Our measurements in 2009 may not fully describe several small sub-events, reflecting only the cumulative displacement caused by the three or more consecutive events (Figure 10). Given differences between the 2009 event and earlier events, it may not be appropriate to define a single recurrence interval. Future studies will be required to assess the consistency of these events.

7. Conclusions

[28] We developed a SSE detection approach that includes both positionogram and parameter estimation methods, which worked well for the Nicoya peninsula' noisy data. We detected five significant events during the period of 2002 to 2011, indicating an average SSE recurrence interval of 21 ± 6 months. The recurrence interval we identified in this area is longer than SSE recurrence interval in Cascadia [*Rogers and Dragert*, 2003; *Szeliga et al.*, 2008] and short term SSE in southwest Japan [*Obara*, 2010]. However, given the significant difference between the 2009 event and earlier events, we question the validity of a uniform recurrence interval model for the Nicoya segment of the Middle America Trench. Small SSEs are detected in northern part of the peninsula, with a shorter recurrence interval of ∼1 year. The northern and southern stations exhibit different SSE slip directions. Stations in the southern peninsula have most of their slip in the East-West direction, while northern stations (HATI, PNEG, SAJU and GRZA) have relatively larger North-South slip.

[29] Our noise analysis results show daily observation noise of 2 mm for horizontal components, significantly smaller than surface displacement of SSE. *Liu et al.* [2007] suggested that three slow slip events in Mexico were trigged by earthquakes

inland. However, no such inland earthquakes occurred during the time of the SSEs in Nicoya, suggesting our events were not similarly triggered.

[30] Slow slip events may impact the size and timing of future earthquakes. If the approximately two year recurrence interval that we observe between 2002 and 2011 is typical of the entire seismic cycle, and if these events are similar to the 2007 event, equivalent to a moment magnitude 6.6 ~ 7.2 earthquake, then significant strain will be released aseismically, reducing the rupture limit and/or total rupture area of future events. However, the occurrence of these events may "load" adjacent segments of the plate interface and increase seismic hazard in these neighboring segments.

Acknowledgments

[31] This work was supported by National Science Foundation grants OCE0841091 and EAR0842137 to THD, and NASA Earth and Space Science Fellowship NNX09AO62H to YJ. This material is based on data, equipment, and engineering services provided by the UNAVCO Facility with support from NSF and NASA under NSF Cooperative Agreement EAR-0735156. We thank Susan Schwartz and Jake Walter who kindly provided the tremor data in Costa Rica and helpful discussions, and two anonymous reviewers for helpful comments on an earlier version of this manuscript. We thank Charles DeMets for providing the Caribbean plate motion pole in the ITRF2008 reference frame.

References

Aguiar, A. C., T. I. Melbourne, and C. W. Scrivner (2009), Moment release rate of Cascadia tremor constrained by GPS, *J. Geophys. Res.*, *114*, B00A05, doi:10.1029/2008JB005909.

Altamimi, Z., et al. (2011), ITRF2008: An improved solution of the international terrestrial reference frame, *J. Geod.*, *85*, 457–473.

Barckhausen, U., C. R. Ranero, R. von Huene, S. C. Cande, and H. A. Roeser (2001), Revised tectonic boundaries in the Cocos Plate off Costa Rica: Implications for the segmentation of the convergent margin and for plate tectonic models, *J. Geophys. Res.*, *106*, 19,207–19,220, doi:10.1029/2001JB000238.

Beroza, G. C., and S. Ide (2011), Slow earthquakes and nonvolcanic tremor, *Annu. Rev. Earth Planet. Sci.*, *39*(1), 271–296, doi:10.1146/annurev-earth-040809-152531.

Bertiger, W., et al. (2010), Single receiver phase ambiguity resolution with GPS data, *J. Geod.*, *84*(5), 327–337, doi:10.1007/s00190-010-0371-9.

Boehm, J., B. Werl, and H. Schuh (2006), Troposphere mapping functions for GPS and very long baseline interferometry from European Centre for Medium-Range Weather Forecasts operational analysis data, *J. Geophys. Res.*, *111*, B02406, doi:10.1029/2005JB003629.

Bos, M. S., et al. (2008), Fast error analysis of continuous GPS observations, *J. Geod.*, *82*(3), 157–166, doi:10.1007/s00190-007-0165-x.

Brown, J. R., G. C. Beroza, S. Ide, K. Ohta, D. R. Shelly, S. Y. Schwartz, W. Rabbel, M. Thorwart, and H. Kao (2009), Deep low-frequency earthquakes in tremor localize to the plate interface in multiple subduction zones, *Geophys. Res. Lett.*, *36*, L19306, doi:10.1029/2009GL040027.

Brown, K. M., et al. (2005), Correlated transient fluid pulsing and seismic tremor in the Costa Rica subduction zone, *Earth Planet. Sci. Lett.*, *238*(1–2), 189–203, doi:10.1016/j.epsl.2005.06.055.

Davis, E. E., and H. W. Villinger (2006), Transient formation fluid pressures and temperatures in the Costa Rica forearc prism and subducting oceanic basement: CORK monitoring at ODP Sites 1253 and 1255, *Earth Planet. Sci. Lett.*, *245*(1–2), 232–244, doi:10.1016/j.epsl.2006.02.042.

Davis, E., et al. (2011), Evidence for episodic aseismic slip across the subduction seismogenic zone off Costa Rica: CORK borehole pressure observations at the subduction prism toe, *Earth Planet. Sci. Lett.*, *306*(3–4), 299–305, doi:10.1016/j.epsl.2011.04.017.

DeMets, C. (2001), A new estimate for present day Cocos and Caribbean Plate motion: Implications for slip along the Central American Volcanic Arc, *Geophys. Res. Lett.*, *28*(21), 4043–4046, doi:10.1029/2001GL013518.

DeShon, H. R., S. Y. Schwartz, S. L. Bilek, L. M. Dorman, V. Gonzalez, J. M. Protti, E. R. Flueh, and T. H. Dixon (2003), Seismogenic zone structure of the southern Middle America Trench, Costa Rica, *J. Geophys. Res.*, *108*(B10), 2491, doi:10.1029/2002JB002294.

DeShon, H. R., et al. (2006), Seismogenic zone structure beneath the Nicoya Peninsula, Costa Rica, from three-dimensional local earthquake P- and S-wave tomography, *Geophys. J. Int.*, *164*(1), 109–124, doi:10.1111/j.1365-246X.2005.02809.x.

Dixon, T. H. (1993), GPS measurement of relative motion of the Cocos and Caribbean Plates and strain accumulation across the Middle America Trench, *Geophys. Res. Lett.*, *20*(20), 2167–2170, doi:10.1029/93GL02415.

Feng, L., et al. (2010), Interseismic megathrust coupling near Nicoya, Costa Rica between 1994 and 2010, Abstract T44B-05 presented at 2010 Fall Meeting, AGU, San Francisco, Calif., 13–17 Dec.

Hackl, M., R. Malservisi, U. Hugentobler, and R. Wonnacott (2011), Estimation of velocity uncertainties from GPS time series: Examples from the analysis of the South African TrigNet network, *J. Geophys. Res.*, *116*, B11404, doi:10.1029/2010JB008142.

Hill, E. M., J. L. Davis, P. Elósegui, B. P. Wernicke, E. Malikowski, and N. A. Niemi (2009), Characterization of site-specific GPS errors using a short-baseline network of braced monuments at Yucca Mountain, southern Nevada, *J. Geophys. Res.*, *114*, B11402, doi:10.1029/2008JB006027.

Holtkamp, S., and M. R. Brudzinski (2010), Determination of slow slip episodes and strain accumulation along the Cascadia margin, *J. Geophys. Res.*, *115*, B00A17, doi:10.1029/2008JB006058.

Ito, Y., et al. (2007), Slow earthquakes coincident with episodic tremors and slow slip events, *Science*, *315*(5811), 503–506, doi:10.1126/science.1134454.

Jiang, Y., and S. Wdowinski (2008), Position-gram: A visual method for detecting transient events in continuous GPS time series, *Eos Trans. AGU*, *89*(53), Fall Meet. Suppl., Abstract G53C-04.

Jiang, Y., R. McCaffrey, S. Wdowinski, T. Dixon, M. Protti, V. M. Gonzalez, A. V. Newman, and L. Feng (2011), Plate coupling and transient events detection from geodetic

measurements in Nicoya Peninsula, Costa Rica, Abstract S23B-2258 presented at 2011 Fall Meeting, AGU, San Francisco, Calif., 5–9 Dec.

King, M. A., and S. D. P. Williams (2009), Apparent stability of GPS monumentation from short-baseline time series, *J. Geophys. Res.*, *114*, B10403, doi:10.1029/2009JB006319.

LaFemina, P., T. H. Dixon, R. Govers, E. Norabuena, H. Turner, A. Saballos, G. Mattioli, M. Protti, and W. Strauch (2009), Fore-arc motion and Cocos Ridge collision in Central America, *Geochem. Geophys. Geosyst.*, *10*, Q05S14, doi:10.1029/2008GC002181.

Larson, K. M., A. R. Lowry, V. Kostoglodov, W. Hutton, O. Sánchez, K. Hudnut, and G. Suárez (2004), Crustal deformation measurements in Guerrero, Mexico, *J. Geophys. Res.*, *109*, B04409, doi:10.1029/2003JB002843.

Liu, Y., et al. (2007), Seismicity variations associated with aseismic transients in Guerrero, Mexico, 1995–2006, *Earth Planet. Sci. Lett.*, *262*(3–4), 493–504, doi:10.1016/j.epsl.2007.08.018.

Liu, Z., et al. (2010), Estimation of interplate coupling in the Nankai trough, Japan using GPS data from 1996 to 2006, *Geophys. J. Int.*, *181*(3), 1313–1328, doi:10.1111/j.1365-246X.2010.04600.x.

Lundgren, P., M. Protti, A. Donnellan, M. Heflin, E. Hernandez, and D. Jefferson (1999), Seismic cycle and plate margin deformation in Costa Rica: GPS observations from 1994 to 1997, *J. Geophys. Res.*, *104*(B12), 28,915–28,926, doi:10.1029/1999JB900283.

Mao, A., C. G. A. Harrison, and T. H. Dixon (1999), Noise in GPS coordinate time series, *J. Geophys. Res.*, *104*(B2), 2797–2816, doi:10.1029/1998JB900033.

Newman, A. V., S. Y. Schwartz, V. Gonzalez, H. R. DeShon, J. M. Protti, and L. M. Dorman (2002), Along-strike variability in the seismogenic zone below Nicoya Peninsula, Costa Rica, *Geophys. Res. Lett.*, *29*(20), 1977, doi:10.1029/2002GL015409.

Norabuena, E., et al. (2004), Geodetic and seismic constraints on some seismogenic zone processes in Costa Rica, *J. Geophys. Res.*, *109*, B11403, doi:10.1029/2003JB002931.

Obara, K. (2010), Phenomenology of deep slow earthquake family in southwest Japan: Spatiotemporal characteristics and segmentation, *J. Geophys. Res.*, *115*, B00A25, doi:10.1029/2008JB006048.

Okada, Y. (1985), Surface deformation due to shear and tensile faults in a half-space, *Bull. Seismol. Soc. Am.*, *75*(4), 1135–1154.

Outerbridge, K. C., T. H. Dixon, S. Y. Schwartz, J. I. Walter, M. Protti, V. Gonzalez, J. Biggs, M. Thorwart, and W. Rabbel (2010), A tremor and slip event on the Cocos-Caribbean subduction zone as measured by a global positioning system (GPS) and seismic network on the Nicoya Peninsula, Costa Rica, *J. Geophys. Res.*, *115*, B10408, doi:10.1029/2009JB006845.

Peng, Z., and J. Gomberg (2010), An integrated perspective of the continuum between earthquakes and slow-slip phenomena, *Nat. Geosci.*, *3*(9), 599–607, doi:10.1038/ngeo940.

Protti, M., et al. (1995), The March 25, 1990 (M_w = 7.0, M_L = 6.8), earthquake at the entrance of the Nicoya Gulf, Costa Rica: Its prior activity, foreshocks, aftershocks, and triggered seismicity, *J. Geophys. Res.*, *100*(B10), 20,345–20,358, doi:10.1029/94JB03099.

Protti, M., V. Gonzalez, T. Kato, T. Iinuma, S. Miyazaki, K. Obana, Y. Kaneda, P. La Femina, T. Dixon, and S. Schwartz (2004), A creep event on the shallow interface of the Nicoya Peninsula, Costa Rica seismogenic zone, *Eos Trans. AGU*, *85*(87), Fall Meet. Suppl., Abstract S41D-07.

Rogers, G., and H. Dragert (2003), Episodic tremor and slip on the Cascadia subduction zone: The chatter of silent slip, *Science*, *300*(5627), 1942–1943, doi:10.1126/science.1084783.

Schmid, R., et al. (2007), Generation of a consistent absolute phase-center correction model for GPS receiver and satellite antennas, *J. Geod.*, *81*(12), 781–798, doi:10.1007/s00190-007-0148-y.

Schmidt, D. A., and H. Gao (2010), Source parameters and time-dependent slip distributions of slow slip events on the Cascadia subduction zone from 1998 to 2008, *J. Geophys. Res.*, *115*, B00A18, doi:10.1029/2008JB006045.

Schwartz, S. Y., and J. M. Rokosky (2007), Slow slip events and seismic tremor at circum-Pacific subduction zones, *Rev. Geophys.*, *45*, RG3004, doi:10.1029/2006RG000208.

Schwartz, S., J. Kim, J. I. Walter, M. Protti, V. M. Gonzalez, T. H. Dixon, and Y. Jiang (2011), Slow slip and tremor at the northern Costa Rica subduction zone, Abstract S32B-01 presented at 2011 Fall Meeting, AGU, San Francisco, Calif., 5–9 Dec.

Segall, P., et al. (2006), Earthquakes triggered by silent slip events on Kilauea volcano, Hawaii, *Nature*, *442*(7098), 71–74, doi:10.1038/nature04938.

Sella, G. F., T. H. Dixon, and A. Mao (2002), REVEL: A model for Recent plate velocities from space geodesy, *J. Geophys. Res.*, *107*(B4), 2081, doi:10.1029/2000JB000033.

Szeliga, W., T. Melbourne, M. Santillan, and M. Miller (2008), GPS constraints on 34 slow slip events within the Cascadia subduction zone, 1997–2005, *J. Geophys. Res.*, *113*, B04404, doi:10.1029/2007JB004948.

Tryon, M. D. (2009), Monitoring aseismic tectonic processes via hydrologic responses: An analysis of log-periodic fluid flow events at the Costa Rica outer rise, *Geology*, *37*(2), 163–166, doi:10.1130/G25342A.1.

Walter, J. I., S. Y. Schwartz, J. M. Protti, and V. Gonzalez (2011), Persistent tremor within the northern Costa Rica seismogenic zone, *Geophys. Res. Lett.*, *38*, L01307, doi:10.1029/2010GL045586.

Wdowinski, S., Y. Bock, J. Zhang, P. Fang, and J. Genrich (1997), Southern California Permanent GPS Geodetic Array: Spatial filtering of daily positions for estimating coseismic and postseismic displacements induced by the 1992 Landers earthquake, *J. Geophys. Res.*, *102*(B8), 18,057–18,070, doi:10.1029/97JB01378.

Wernicke, B., and J. L. Davis (2010), Detecting large-scale intra continental slow-slip events (SSEs) using geodograms, *Seismol. Res. Lett.*, *81*(5), 694–698, doi:10.1785/gssrl.81.5.694.

Williams, S. D. P. (2003), The effect of coloured noise on the uncertainties of rates estimated from geodetic time series, *J. Geod.*, *76*(9–10), 483–494, doi:10.1007/s00190-002-0283-4.

Zhang, J., Y. Bock, H. Johnson, P. Fang, S. Williams, J. Genrich, S. Wdowinski, and J. Behr (1997), Southern California Permanent GPS Geodetic Array: Error analysis of daily position estimates and site velocities, *J. Geophys. Res.*, *102*(B8), 18,035–18,055, doi:10.1029/97JB01380.

Zumberge, J. F., M. B. Heflin, D. C. Jefferson, M. M. Watkins, and F. H. Webb (1997), Precise point positioning for the efficient and robust analysis of GPS data from large networks, *J. Geophys. Res.*, *102*(B3), 5005–5017, doi:10.1029/96JB03860.